LIMNOLOGY and OCEANOGRAPHY

ASLO

Limnol. Oceanogr. 67, 2022, 713–725

doi: 10.1002/lno.12031

Optical determinations of photophysiology along an ecological gradient in the North Pacific Ocean

James G. Allen [1,2*] **Mathilde Dugenne** [1,2] **Ricardo M. Letelier,** [3] **Angelicque E. White** [1,2]

[1]Department of Oceanography, School of Ocean and Earth Science and Technology, University of Hawai'i at Mānoa, Honolulu, Hawai'i

[2]Daniel K. Inouye Center for Microbial Oceanography: Research and Education, University of Hawai'i at Mānoa, Honolulu, Hawai'i

[3]College of Earth and Oceanic Sciences, Oregon State University, Corvallis, Oregon

Abstract

Photosynthesis acts as a fundamental control in the cycling of biologically reactive elements in the ocean. Modeling photosynthesis requires an understanding of its response to light, specifically the maximum rate of photosynthesis per photon absorbed and the irradiance level at which it becomes light-saturated (E_k), though field measurements of these parameters are both time and labor intensive. As absorbed light either drives photosynthesis, is re-emitted as fluorescence, or is converted to heat, fluorescence can be related to the photosynthetic response to light in that, as light increases, there exists an inflection point where the probability that excess absorbed energy is dissipated as heat increases and fluorescence yield is decreased. Accordingly, we use a combination of in vivo chlorophyll fluorescence, particulate matter absorption spectra, and photosynthetically active radiation measurements to approximate this inflection irradiance (termed E_{FT}) and relate it to modeled E_k along a transect from the oligotrophic North Pacific Subtropical Gyre to the edge of the more eutrophic subpolar gyre (~ 45°N). We find that E_{FT} declines by a factor of 4× from values of 200–300 μmol photons m^{-2} s^{-1} in the oligotrophic gyre to 50–100 μmol photons m^{-2} s^{-1} north of the transition zone and correlates well with E_k from traditional data and models. This latitudinal pattern is associated with changes in biomass concentrations and the phytoplankton carbon to chlorophyll ratio, as well as with changes in particulate carbon to nitrogen ratios. Collectively, these results demonstrate a promising framework to capture high-resolution variability in a key photosynthetic parameter.

Ocean ecosystems play a central role in the global carbon cycle, with global primary production by phytoplankton photosynthesis averaging on the order of ~ 50 Pg C yr^{-1} (Sathyendranath et al. 2019). At any given depth within the euphotic layer, the absolute rate of photosynthesis is driven by the time-variant flux of solar irradiance and its absorption by the photosynthetic pigments of phytoplankton, the biomass of which is determined by the availability of essential nutrients and mortality terms such as grazing and viral lysis. The dependence of light absorption and its conversion into photosynthate on irradiance—photosynthesis vs. irradiance or P-I—is fundamental to the description of marine primary production (Wallen and Geen 1971; Edwards et al. 2016); it is classically measured from carbon uptake experiments over a range of irradiances, termed P-I experiments (Lewis and Smith 1983; Bouman et al. 2018). The light response curve of phytoplankton photosynthesis generally follows a hyperbolic relationship (Jassby and Platt 1976) with photosynthetic rates proceeding as a linear function of irradiance at low light with a slope defined as either a function of incident or absorbed light (Behrenfeld et al. 2004). At some irradiance level, photosynthesis becomes light-saturated and proceeds at maximal rates unless photoinhibition occurs. Both the initial slope and the maximum photosynthetic rate vary as a function of irradiance regime, nutrient supply, and temperature, reflecting both acclimation (Geider et al. 1996) and stress (Platt et al. 1992; Babin et al. 1996). When rates are normalized to the concentration of the light harvesting pigment chlorophyll (Chl) *a*, the initial slope of the light response curve is a function of the absorption cross-section of photosynthetic pigments relative to chlorophyll and the maximum efficiency of photochemical conversion of light to carbon, whereas the maximum photosynthetic rate is a function of the concentration or activity of the Calvin cycle enzyme RUBISCO relative to chlorophyll

*Correspondence: jgallen@hawaii.edu

Additional Supporting Information may be found in the online version of this article.

(Platt and Jassby 1976; Geider and MacIntyre 2002). A thorough and detailed description of these terms and the factors that drive them to vary is described in Behrenfeld et al. (2004) and references cited therein.

Photosynthesis vs. irradiance experiments, though time- and labor-intensive, have proven critical to parameterize biogeochemical and optical models of marine primary production (Harrison et al. 1985; Uitz et al. 2008; Kulk et al. 2020). In a meta-analysis of more than 5000 P-I experiments, Bouman et al. (2018) compared the chlorophyll-normalized maximum photosynthetic rate and the initial slope with increasing irradiance across ecological provinces and found a strong positive correlation between these parameters. Furthermore, they determined that the ratio of the maximum rate and the initial slope, referred to as the light saturation parameter for photosynthesis, E_k, ranges between ~ 20–300 μmol photons m^{-2} s^{-1} as a function of latitude: high latitudes (> 65°N) are characterized by a mean E_k value of ~ 60 μmol photons m^{-2} s^{-1}, while low latitudes (40°S–40°N) have an average E_k value of ~ 150 μmol photons m^{-2} s^{-1} in the surface layer. The positive correlation between the maximum rate of photosynthesis and its initial slope is attributed to physiological factors such as changes in the allocation of ATP and NADPH as well as ecological factors including changes in phytoplankton community composition as described by Behrenfeld et al. (2004) and Côté and Platt (1983). The observed latitudinal variability in E_k was hypothesized to be related to either temperature or light controlled changes in the concentration (i.e., intraspecific photoacclimation) and composition (i.e., interspecific photoadaptation) of photosynthetic pigments (Bouman et al. 2018).

Patterns in phytoplankton responses to light and associated changes in production have also been assessed by examination of the dynamics of chlorophyll fluorescence (Kiefer and Reynolds 1992; Kolber and Falkowski 1993; Jolliff et al. 2012). Briefly, phytoplankton acclimate to the ambient light field by modifying cell-specific pigment concentrations which in turn alter overall absorption efficiency, fluorescence yield per chlorophyll, and the chlorophyll to carbon ratio (Geider et al. 1998; Roesler and Barnard 2013). Changes in fluorescence yield, the amount of absorbed light energy reemitted as fluorescence, can be related to photosynthesis, as light is either used to drive photosynthesis, emitted as fluorescence, or converted to heat (Butler and Strasser 1977; Cullen et al. 1997; Falkowski and Raven 2007). The three fates of absorbed light energy are therefore competing processes with their relative proportions changing, for example, over a diel cycle.

In an irradiance-based model to quantify the photochemical and nonphotochemical quenching of fluorescence, Morrison (2003) describes an inflection irradiance or fluorescence threshold, E_{FT}, at which the fluorescence yield begins to decrease with increasing irradiance. To characterize this threshold, Comeau (2010) used moored and profiling conductivity, temperature, and depth (CTD) package data to monitor the ratio of chlorophyll fluorescence relative to the chlorophyll concentration determined via line-height absorption (Chl_{fl} : Chl_{a676}) as a function of light. At very low light levels, a greater proportion of light energy is being used to drive photochemistry and the fluorescence yield increases with irradiance up to E_{FT} due to the decreased probability of photochemical quenching (Kiefer and Reynolds 1992), with a relatively high Chl_{fl} : Chl_{a676}. As light becomes saturating for photosynthesis and passes the fluorescence inflection point, phytoplankton begin to dissipate excess absorbed energy as heat, and Chl_{fl} : Chl_{a676} will significantly decrease, a process termed nonphotochemical quenching. This diel pattern in nonphotochemical quenching has been shown to strongly correlate with important primary production parameters such as the photosynthetic efficiency and electron requirement for carbon fixation by phytoplankton (Schuback and Tortell 2019). Characterizing photochemical and nonphotochemical quenching as a function of irradiance can provide valuable in situ information on the photo-acclimation patterns of sea surface phytoplankton assemblages required in the interpretation of solar induced fluorescence derived from ocean color remote sensing (Behrenfeld et al. 2009). Roesler and Barnard (2013) presented a framework for investigating this ratio simply by measuring in vivo chlorophyll fluorescence, the line-height chlorophyll absorption at 676 nm, and photosynthetically active radiation (PAR), albeit this has not been assessed across basin-scale environmental and ecological gradients.

Here, we utilize a unique set of continuous sensors to simultaneously resolve phytoplankton optical properties, plankton size and diversity, and biological production across several ecotones spanning the North Pacific Ocean as part of the Simons Collaboration on Ocean Processes and Ecology Gradients campaign. The approach, developed by Comeau (2010), was used to derive E_{FT} from underway observations of PAR, chlorophyll fluorescence, and chlorophyll line height absorption along the transect. The objective of this study was to characterize changes in the photophysiological characteristics of phytoplankton communities with a high resolution and autonomous approach and relate them to corresponding changes in plankton biomass, elemental composition, and community production across a latitudinal gradient.

Methods

In April 2019, we conducted a latitudinal transect along 158°W from Honolulu, Hawaii, to 42.3°N aboard the *R/V Kilo Moana* (KM1906, *Gradients 3* campaign, www.simonscmap.com/catalog/cruises/KM1906, Fig. 1). The aim of the survey was to understand the drivers of latitudinal changes in elemental composition, plankton community structure, and primary production across an ecological gradient from the oligotrophic North Pacific Subtropical Gyre (NPSG) to the transition zone bordering the nutrient-rich subpolar gyre of the Pacific Ocean (Juranek et al. 2020). Near-continuous optical measurements of

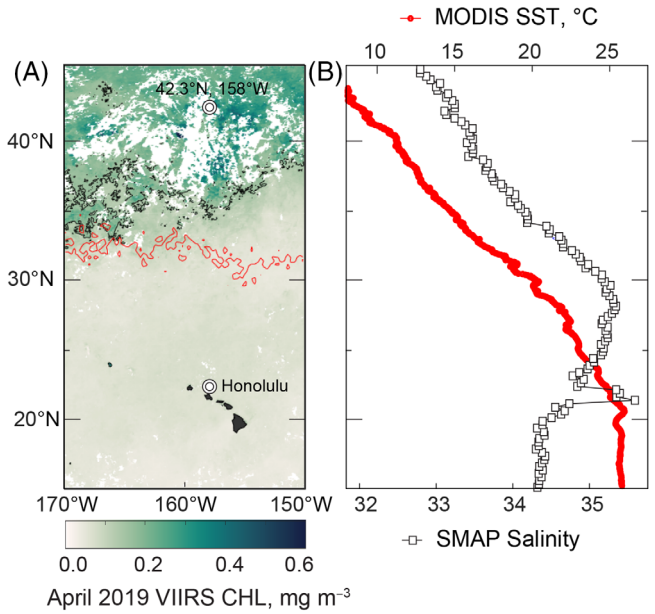

Fig. 1. (**A**) Satellite retrievals of chlorophyll concentration for the month of April 2019 using the OCI algorithm on VIIRS. Shown in red is the 34.82 surface isohaline corresponding to the southern edge of the transition zone, while the black line corresponds to the chlorophyll isoline value of 0.15 mg m^{-3} corresponding to the transition zone chlorophyll front. The cruise track departed Honolulu, Hawaii along 158°W and reached a northernmost latitude of 42.3°N before transiting southward. (**B**) Latitudinal values of MODIS-derived sea surface temperature (°C, red circles) and SMAP-derived salinity values (PSU, white squares) along the transect at 158°W for April 2019.

hyperspectral absorption and attenuation, particulate beam transmission, particulate backscattering, and chlorophyll fluorescence in near-surface waters were conducted between 09 April and 30 April 2019, using the ship's underway flow-through system (~ 7 m depth inlet). In addition, discrete measurements were conducted regularly underway and at nine stations along this gradient, and seawater was collected daily for net community production incubations. Methodological details are presented below.

Discrete measurements

Particulate carbon and particulate nitrogen concentrations (n = 470) were determined from discrete water samples (between ~ 2 and ~ 6 liters) collected from the ship's uncontaminated seawater system and filtered onto precombusted glass fiber filters every ~ 2.5 h using a semi-automated filtration device based on the design of Holser et al. (2011). Particulate carbon was determined via high temperature combustion as per the HOT protocols (www.hahana.soest.hawaii.edu/hot/methods/pcpn.html, Sharp 1974) with acetanilide as an internal standard. All samples were corrected to remove dry filter blanks and contribution of dissolved organic carbon is assumed to be negligible.

Discrete samples for Chl a concentration (~ 0.5 liters, n = 16) were taken from the inline underway system and from the surface bottles of the CTD rosette for multiple stations along the transect. Samples were collected onto glass fiber filters (GF/F) and measured using a Turner Designs Model 10-AU fluorometer using standard methods described in Strickland and Parsons (1972) modified to use 100% acetone as the solvent (Bowles et al. 1985). Nitrate plus nitrite ($NO_3 + NO_2$ or simply referred to as nitrate) as well as phosphate (soluble reactive phosphorus, PO_4) samples were collected daily (n = 65) from the underway flow through system as well as the CTD-rosette and analyzed using a SEAL Analytical AutoAnalyzer III following procedures documented in Strickland and Parsons (1972) and described in Juranek et al. (2020). The detection limit is 75 nmol L^{-1} for $NO_3 + NO_2$ and 30 nmol L^{-1} for PO_4.

Underway measurements of phytoplankton biomass and production

Phytoplankton abundance and carbon content was measured by a pair of continuous flow cytometers: the SeaFlow (Swalwell et al. 2011), which detects auto-fluorescing particles ranging in size from ~ 0.4 to ~ 6 μm, and the Imaging FlowCytobot (IFCB; Olson and Sosik 2007) which images 4–100 μm particles detected on both scattering and auto-fluorescence. We used a subset of the IFCB dataset, including only auto-fluorescing particles, to determine the phytoplankton biomass in the 4–100 μm size range. Phytoplankton carbon was derived from direct estimates of particulate biovolume from the IFCB (Moberg and Sosik 2012) and the application of Mie Theory to convert forward light scatter measured by the SeaFlow into biovolume, as described in Ribalet et al. (2019). All biovolume estimates were then converted to carbon using allometric scaling (Menden-Deuer and Lessard 2000). Additional details of data processing are described in Juranek et al. (2020). These data are used here to validate our estimate of phytoplankton carbon. Measurements of net community production (mmol O_2 m^{-2} d^{-1}) were derived from continuous measurements of O_2/Ar in the surface mixed layer as described and presented in Juranek et al. (2020). These data are shown here for reference to latitudinal changes in E_{FT} and proxies of photoacclimation.

Underway optics and hydrography

The ship's thermosalinograph system, comprised of an SBE-38 remote temperature sensor located at the seawater intake situated ~ 7 m below the sea surface in conjunction with an SBE-45 analog thermosalinograph sensor placed in a sea chest near the bow of the ship, was utilized for measurement of sea surface temperature (°C) and salinity (PSU). Uncontaminated seawater samples from the same intake were delivered to the ship's wet laboratory in the dark using the ship's March Model TE-8K-MD magnetic drive pump, rated at 400 L m^{-1} with an estimated delay on the order of ~ 10 s.

Continuous underway optical measurements were made using an AC-S operating in benchtop mode in line with an ECO Triplet (SeaBird, Philomath, Oregon), housed in a 7.6-cm

diameter PVC chamber with a highly absorbing black interior. For the first 10 min of every hour, incoming seawater was passed through a 0.2 μm filter (Graver ZTEC G series with Teflon O-rings) to collect dissolved "blanks" that were subsequently used to correct whole-water signals from both the AC-S and the ECO Triplet collected in the succeeding 50 min of each hour. This allowed for the establishment of a relative calibration of the instruments and minimized the influence of biofouling. Filtered values were linearly interpolated throughout the cruise and subtracted from raw measurements to provide in vivo chlorophyll fluorescence (volts, excitation/emission = 470/695 nm), the particulate volume scattering function at 700 nm at 117° (volts), spectral particulate beam attenuation at 83 wavelengths (m^{-1}), and spectral particulate absorption at 83 wavelengths (m^{-1}). Voltage measurements from the ECO sensor were then scaled to particulate volume scattering values (m^{-1} sr^{-1}) using factory calibrations. In vivo fluorescence-derived chlorophyll (Chl_{fl}) was calculated from raw voltage by calibrating to discrete extracted chlorophyll measurements ($n = 16$) collected at nighttime with a slope of 0.0025 mg m^{-3} V^{-1} and a r^2 of 0.94. The use of a single calibration coefficient for the transect was determined to be sufficient as E_{FT} was calculated relative to the closest low-light values and is explained in more detail in the next section. Particulate volume scattering at 117° (β_p) was converted to the hemispherical particulate backscattering coefficient (b_{bp}, m^{-1}), following Boss and Pegau (2001):

$$b_{bp} = 2\pi\chi_p\beta_p \quad (1)$$

where the conversion factor χ_p is 1.1 for 117° (Boss and Pegau 2001). An initial quality control for the AC-S measurements removed negative particulate beam attenuation and absorption spectra and any spectra with a slope greater than three standard deviations of the hourly average to account for bubbles or large, rare particles. Particulate absorption was then corrected for residual temperature and scattering after Slade et al. (2010). The dissolved component of absorption was calculated from filtered measurements using a Nanopure freshwater blank and temperature and salinity corrected according to Slade et al. (2010).

Calculations of the diffuse attenuation coefficient of PAR from the surface to the 7 m depth of the underway intake, described below, require both total absorption and total backscattering coefficient spectra. As the underway protocol provides relatively calibrated particulate optical data to reduce biofouling, modeled seawater absorption and backscattering spectra are derived to be added to observations of particulate optics. The total spectral absorption coefficient (m^{-1}) was calculated by adding the absorption by pure seawater after Mason et al. (2016) between 400 and 550 nm, and Pope and Fry (1997) from 550 to 700 nm to the sum of the dissolved and particulate absorption spectra. Total particulate backscattering spectra were calculated by extrapolating the ECO particulate backscattering value, calculated at 700 nm, to all AC-S wavelengths assuming a power law slope of 1.0337 (Maritorena et al. 2002). Seawater backscattering was derived from salinity and temperature measurements via Zhang et al. (2009) and added to the particulate backscattering spectra to calculate the total backscattering spectra.

AC-S-derived Chl *a* concentrations (Chl_{a676}) were estimated from the particulate absorption coefficients using the line-height method (Davis et al. 1997; Roesler and Barnard 2013). A chlorophyll-specific absorption coefficient of 0.012 m^2 mg^{-1} was determined from a linear regression of line-height absorption at 676 nm against discrete chlorophyll samples collected across all regions from the underway system within ± 30 min of optical measurements ($n = 16$) and was highly significant (slope = 1.006, $r^2 = 0.98$). Continuous phytoplankton carbon, $C_{PHYTO\text{-}BUCK}$ (mg C m^{-3}), was additionally calculated from Chl_{a676} using the relationship derived in Buck et al. (1996):

$$\log_{10}C_{PHYTO-BUCK} = 1.92 + 0.69\log_{10}Chl_{a676} \quad (2)$$

where the log–log regression against discrete SeaFlow + IFCB phytoplankton carbon data ($n = 373$) was also significant (slope = 0.91, $r^2 = 0.83$).

Photophysiology calculations

Measurements of surface planar PAR (400–700 nm) were made using a LICOR LI-190R quantum cosine collector, logged throughout the day, and averaged in 1 min intervals (data logger model LI-1500). The sensor was positioned 4 m above the deck to minimize the influence of shadows from the ship's superstructure. The diffuse attenuation coefficient for PAR, K_{PAR}, was calculated according to methods described in Lee et al. (2005), which calculates the average K_{PAR} as a function of the solar zenith angle, the total absorption coefficient at 490 nm, and the total backscattering coefficient at 490 nm. Assuming a well-mixed layer above the ship's water intake, the scalar PAR at 7 m depth was then calculated as per Eq. 3 where 1.2 is a conversion factor between downwelling planar PAR and scalar PAR, τ is the transmission PAR between the air–sea interface, and z is 7 m.

$$PAR(7\,m) = 1.2\tau PAR_{surf}e^{-K_{PAR}z} \quad (3)$$

The transmission of PAR through the air–sea interface was calculated according to methods described in Mobley and Boss (2012), which calculates τ as a function of average wind speed and solar zenith angle, assuming clear skies and open-ocean chlorophyll concentrations. Wind speeds were acquired using an RM Young anemometer located on the weather deck of the ship, and sun angles were calculated using time and GPS coordinates.

The fluorescence threshold irradiance, E_{FT}, was approximated using a nonlinear curve function to characterize where ECO Triplet chlorophyll fluorescence (Chl_{fl}) significantly diverges from AC-S line height chlorophyll (Chl_{a676}) as a

function of PAR(7 m) values. To maximize spatial and temporal resolution, measurements of Chl_{fl} : Chl_{a676} were divided into two daily portions: from sunrise to solar noon, and from solar noon to sunset. A nonlinear curve fitting routine described in Comeau (2010) was used to fit two intersecting lines with a Boolean operator to solve for E_{FT}:

$$\begin{aligned} &Chl_{fl} : Chl_{a676} \\ &\quad = (Chl_{fl} : Chl_{a676o}[PAR < E_{FT}]) \\ &\qquad + \left(\left(Chl_{fl} : Chl_{a676o} + m\ln\left(\frac{PAR}{E_{FT}}\right)[PAR \geq E_{FT}]\right)\right) \end{aligned} \quad (4)$$

where the ratio Chl_{fl} : Chl_{a676} is assumed to be constant under low irradiance less than E_{FT} and decreases with a slope m once PAR is greater than E_{FT}. This is expressed via the Boolean operators [PAR < E_{FT}] and [PAR ≥ E_{FT}]), which signify the portions of the function below and above the E_{FT} PAR value, respectively. An example of this curve fitting routine is shown below in Fig. 4. The original Comeau (2010) routine allowed for a significant slope when [PAR < E_{FT}], but here we assume the slope to be null. This same approach has been used to describe the threshold and dose-dependent reduction of viability in phytoplankton exposed to ultraviolet radiation (MacIntyre et al. 2018). The cost function was minimized by the Levenberg–Marquardt nonlinear least squares algorithm with an initial guess of 1 (unitless), −0.4 (μmol photons m^{-2} $s^{-1})^{-1}$, and 200 μmol photons m^{-2} s^{-1} for Chl_{fl} : Chl_{a676o}, m, and E_{FT}, respectively. Confidence intervals were determined using an asymptotic normal distribution for the parameter estimate from the residuals and the Jacobian of the nonlinear function fit in MATLAB (nlparci.m), and poor fits were rejected if their confidence intervals crossed null.

The same approach was used to estimate E_{FT} from the chlorophyll fluorescence emitted by the most abundant group of pigmented cells detected with the IFCB. The laser-induced (635 nm, 4.5 mW) red autofluorescence (680 ± 30 nm, arbitrary units) emitted by individual cells was measured using a photomultiplier (PMT) module (Hamamatsu HC120-05 modified for current-to-voltage), as described in Olson and Sosik (2007). For 24 h, the fluorescence per cell of the main nanophytoplankton group was extracted with a temporal resolution of ~ 20 min (determined by the fixed flow rate of 0.25 mL min^{-1} for the instrument) in two stations located at 30.8°N and 41.3°N along the 158°W transect. The average fluorescence per cell was normalized to cell biovolume to account for changes in biomass over the diel cycle and plotted against the underway PAR values to fit Eq. 4 with initial parameters of 0.6 a.u., −0.4 (μmol photons m^{-2} $s^{-1})^{-1}$, and 200 μmol photons m^{-2} s^{-1}. The instrument settings were kept constant throughout the cruise, as described in Juranek et al. (2020). Standard beads (6 μm, AlignFlow™, molecular probes, excitation: 630–660 nm) were monitored in each sample to detect any instrumental drift, but the regression of beads' red fluorescence against time did not yield a significant slope (n = 1858, intercept = 0.81 a.u.). Similarly, we tested the effect of the relatively long (maximum of 20 min) duration of each analysis, where individual cells intercept the laser in random order at a frequency of 800 kHz by regressing the time of interception against cell fluorescence. In daytime samples especially, cells may have relaxed nonphotochemical quenching as they were kept in the dark from the moment the sample was drawn from the underway inlet to the end of the analysis. However, the regression of cell fluorescence against time for each sample did not yield a significant slope (*see* Supplementary Material). All underway data are accessible on Zenodo.org (doi:10.5281/zenodo.5178648).

Results and discussion

Latitudinal trends in oceanographic conditions

Oceanographic measurements made over the course of the cruise showed a marked transition from typical low-nutrient, low-biomass subtropical surface water masses to the colder, more productive transition zone (Fig. 1). The regional hydrography from this cruise is described in Juranek et al. (2020). Briefly, chlorophyll concentrations increase by a factor of five and net community production estimates increase three- to five-fold between the subtropics and the subpolar region, and high-resolution optical observations suggest that picoeukaryotes and nanoplankton dominate changes in biomass to the north. The area covered by the cruise is divided into three regions, with the boundary between the subtropical gyre and the southern edge of the transition zone defined by the 34.8 surface isohaline (Roden 1971; Lynn 1986), which was located at 32.34°N. Within the transition zone, we follow the convention of Juranek et al. (2020) and define a northern and southern subregion separated by the seasonally variable transition zone chlorophyll front (as defined by the 0.15 mg m^{-3} chlorophyll isoline); this front was positioned at ~ 35°N during the cruise.

The availability of nutrients can play a large role in the variation of photosynthetic parameters such as the initial rate of increasing photosynthesis with irradiance (Platt et al. 1992; Babin et al. 1996; Moore et al. 2008), though care should be taken on the interpretation of nutrient stress on phytoplankton photophysiology (Parkhill et al. 2001). Nutrient analysis at the surface showed that $NO_3 + NO_2$ concentrations were extremely low (at or below detection limit of 75 nmol L^{-1}) until north of ~ 38°N, where concentrations increased to ~ 6.5 μmol L^{-1} at the highest latitudes. Concentrations of PO_4 began increasing above the detection limit (30 nmol L^{-1}) at a much lower latitude, just north of the transition zone boundary, around 33–34°N. Importantly, iron was likely not limiting at the time of our sampling based on a null response to iron addition experiments (N. Hawco pers. comm.).

The subtropical gyre was marked by low biomass and low production, with phytoplankton carbon biomass of 10–15 mg m^{-3} and net community production values of 6–7 mmol O_2 m^{-2} d^{-1}. In the southern portion of the

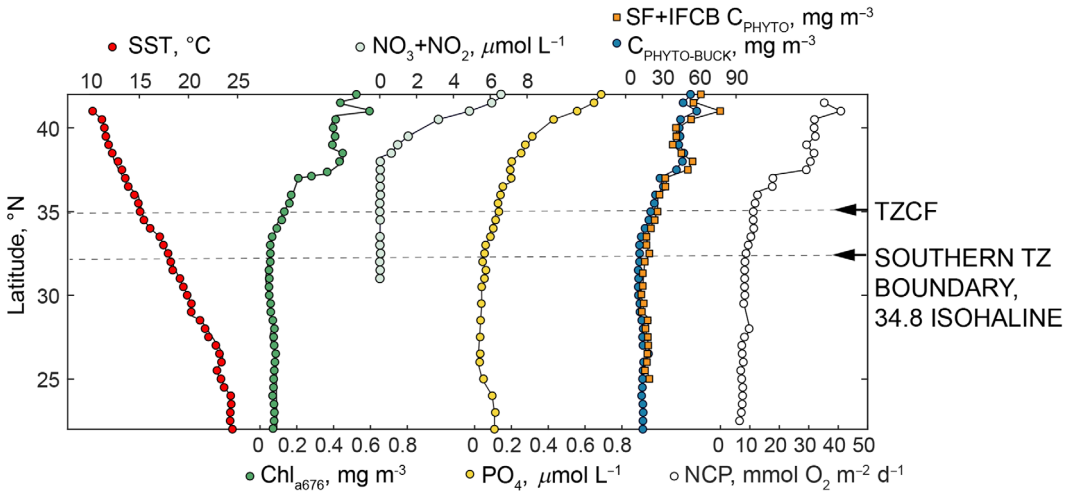

Fig. 2. Latitudinal measurements of sea surface temperature (SST, °C), AC-S derived Chl *a* concentrations (Chl_{a676}, mg m^{-3}), nitrate + nitrite concentrations ($NO_3 + NO_2$, μmol L^{-1}), phosphate concentrations (PO_4, μmol L^{-1}), phytoplankton carbon derived from the AC-S ($C_{PHYTO\text{-}BUCK}$, mg m^{-3}) and from SeaFlow + Imaging FlowCytobot measurements (SF + IFCB C_{PHYTO}, mg m^{-3}), and Net Community Production (NCP, mmol O_2 m^{-2} d^{-1}). The location of the southern boundary of the transition zone as identified via the 34.8 isohaline and the transition zone chlorophyll front (TZCF) are shown as dotted lines.

transition zone below the chlorophyll front, phytoplankton carbon obtained from the sum of measurements made by the SeaFlow and the Imaging FlowCytobot (SF + IFCB C_{PHYTO}) increased to values of 15–25 mg m^{-3}, while net community production nearly doubled to values of 10–12 mmol O_2 m^{-2} d^{-1}. The highest biomass and production values were found north of the chlorophyll front, with values of 75 mg m^{-3} and 40 mmol O_2 m^{-2} d^{-1}, respectively. An optical proxy for phytoplankton carbon ($C_{PHYTO\text{-}BUCK}$), determined with a power law relationship using chlorophyll concentrations (Buck et al. 1996), was well correlated with discrete carbon estimates (log–log fit: slope = 0.913, r^2 = 0.83, n = 373), and showed nearly identical trends in biomass as flow cytometry (SF + IFCB C_{PHYTO}, Fig. 2). The increase of net community production and biomass south of detectable surface nitrate concentrations (within a zone of residual phosphate, ~ 0.25 μmol L^{-1}) suggests prior delivery of nutrients and subsequent utilization.

Temporal variability of phytoplankton biomass and incoming PAR

Bio-optical proxies for biomass and light harvesting pigments in the surface mixed layer were collected across the entire transect to provide insight into the latitudinal variability in photophysiological characteristics of phytoplankton communities (Fig. 3). As expected, incoming solar radiation varied with cloud-cover, particle concentration, and latitude: instantaneous PAR values estimated at a 7 m water depth south of the transition zone chlorophyll front reached up to ~ 1300 μmol photons m^{-2} s^{-1} (Fig. 3A) declining to maxima of ~ 1000 μmol photons m^{-2} s^{-1} to the north. After 3 d at the northern station, a storm forced a temporary transect southward to ~ 33°N from 19 to 23 April, after which the ship returned to the northernmost station before undertaking the southern transit back to Honolulu, Hawaii. Cloudy days were more prevalent in this portion of the cruise, with PAR(7 m) values at solar noon as low as 500–600 μmol photons m^{-2} s^{-1}. The estimates of phytoplankton carbon biomass (Fig. 3B) and chlorophyll derived from AC-S line-height measurements (Fig. 3C) show an increase in biomass beginning at the chlorophyll front.

Photophysiology

At high irradiances, phytoplankton exhibit nonphotochemical quenching of chlorophyll fluorescence, where excess light energy is dissipated as heat loss (Morrison 2003). This is shown clearly in Fig. 3D,E across all regions, where chlorophyll fluorescence and its ratio with absorption-based chlorophyll concentration sharply decreases at midday by up to ~ 50% of the night-time values. Previous studies have shown that the light level at which in vivo chlorophyll fluorescence diverges from absorption-based estimates of chlorophyll is strongly correlated to the saturation irradiance of photosynthesis, E_k (Comeau 2010; Roesler and Barnard 2013). The degree of nonphotochemical quenching has also shown strong correlations with important primary production parameters such as the functional absorption cross section and efficiency of charge separation of photosystem II as well as the electron requirement of carbon fixation (Schuback and Tortell 2019), and is subsequently a powerful diagnostic for the photophysiological state of in situ phytoplankton communities.

Figure 4A,B shows examples of how the quenched chlorophyll fluorescence signal can be mapped to the relatively constant chlorophyll absorption measurements as a function of

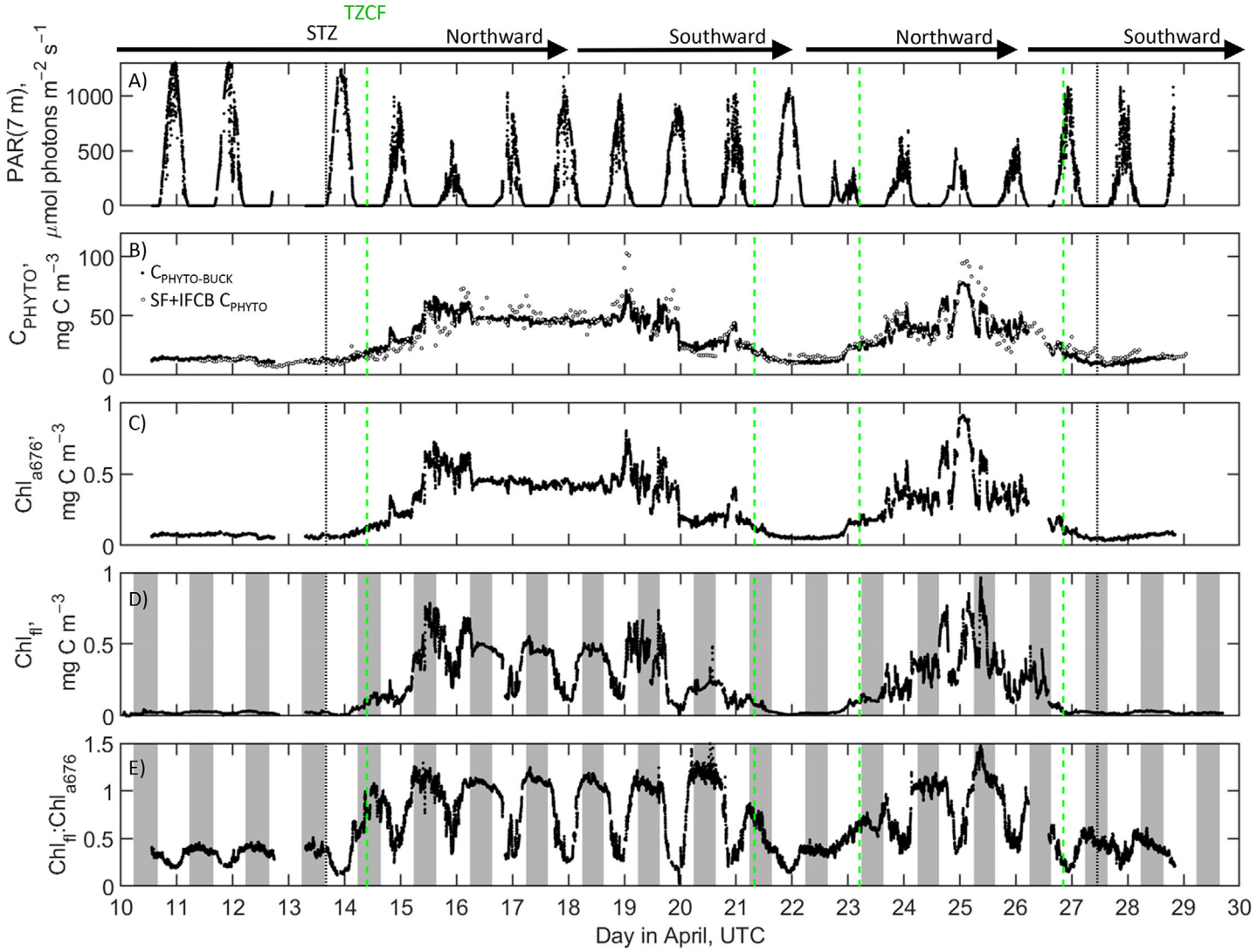

Fig. 3. Time series observations of (**A**) derived scalar photosynthetically available radiation at 7 m depth (PAR(7 m), μmol photons m^{-2} s^{-1}), (**B**) phytoplankton carbon derived from the sum of SeaFlow and Imaging FlowCytobot (SF + IFCB C_{PHYTO}, solid black points) measurements as well as the Buck et al. algorithm ($C_{PHYTO\text{-}BUCK}$, open circles) in units mg C m^{-3}, (**C**) ACS-derived chlorophyll *a* concentrations (Chl_{a676}, mg m^{-3}), (**D**) ECO chlorophyll fluorescence (Chl_{fl}, mg m^{-3}), and (**E**) the ratio of ECO chlorophyll fluorescence and ACS-derived Chl *a* concentrations (Chl_{fl} : Chl_{a676}, unitless). Shaded areas in (**D**) and (**E**) correspond to nighttime measurements, while the black dashed line indicates the crossing of the southern boundary of the transition zone (STZ) and the green dashed line shows the position of the transition zone chlorophyll front (TZCF). The ship's heading (northward or southward) is noted above panel (**A**).

the ambient light to approximate the inflection point at which photosynthesis becomes saturated and excess energy is dissipated as heat, leading to a quenching in the fraction of absorbed light reemitted as fluorescence. Here, the calibrated Chl_{fl} : Chl_{a676} ratio as a function of PAR(7 m) are shown for a low latitude and a high latitude region. In Fig. 4C,D, the same signal can be found for IFCB fluorescence normalized to biovolume, measured for the main population of nanophytoplankton found in a northern and southern region. In all cases, the normalized fluorescence signal is the highest at low light levels while remaining relatively constant, and then decreases when light levels are high enough to induce nonphotochemical quenching, caused by excess dissipation of absorbed energy as heat. The bilinear fit to log-transformed data are shown here for the high and low latitudes for both sets of instruments in linear space (Eq. 4), and the irradiance value for the fluorescence threshold, E_{FT}, the point where both lines meet, is determined with confidence intervals. In addition to the observed higher E_{FT} threshold, low-latitude stations also exhibit a significantly lower maximum Chl_{fl} : Chl_{a676} ratio under light limiting conditions ($PAR < E_{FT}$), suggesting potential differences in light adaptation, photophysiology, and/or taxonomy (Kiefer 1973; Cleveland and Perry 1987). Though the temporal resolution for the IFCB measurements is limited (~ 20 min resolution), the results here demonstrate an avenue for future research.

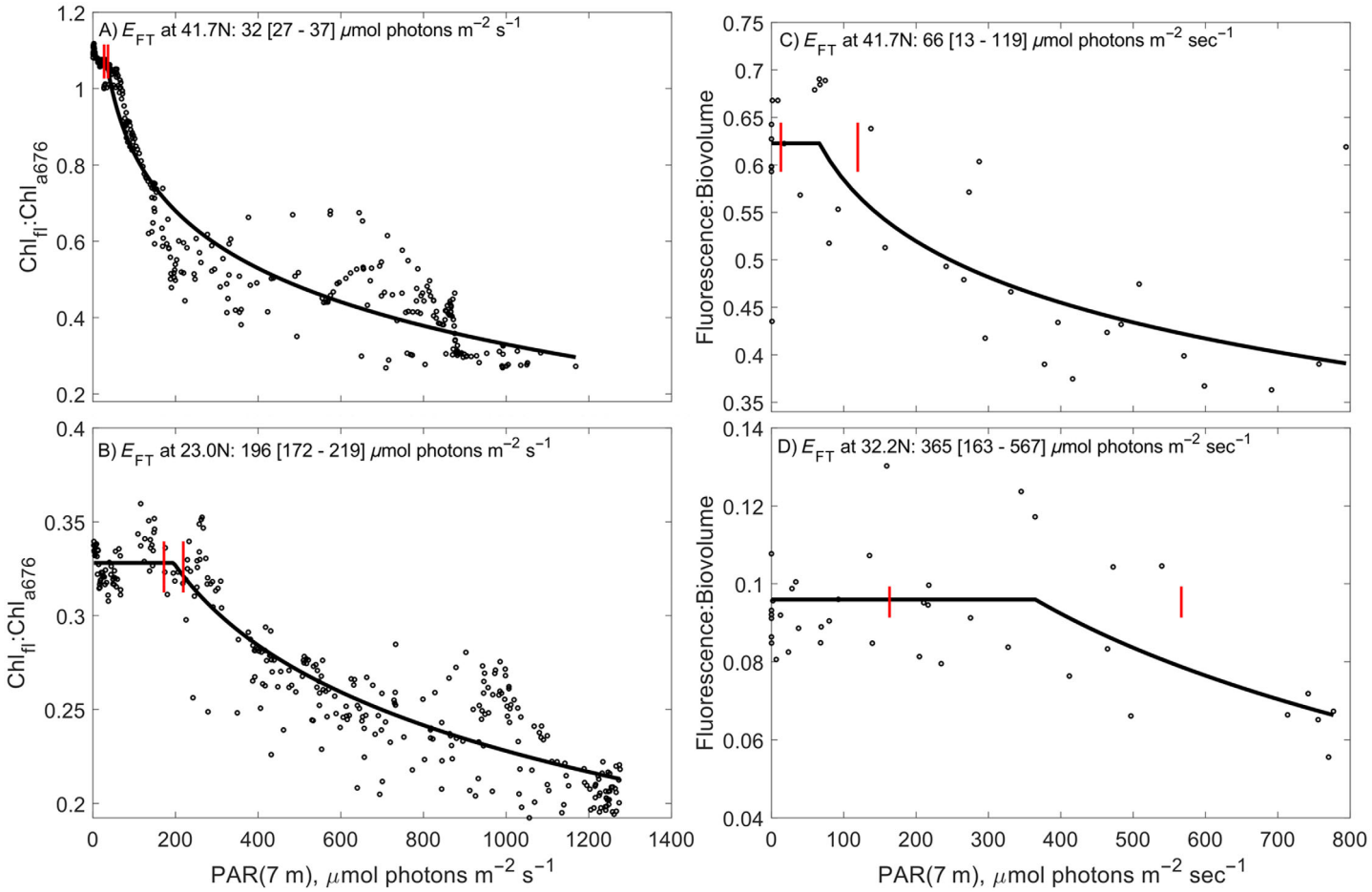

Fig. 4. Observations of the ratio of Chl *a* fluorescence (Chl$_{fl}$) at 7 m from the ECO Triplet to the AC-S line height chlorophyll concentration (Chl$_{a676}$) as a function of PAR calculated at 7 m depth (PAR(7 m)) with the nonlinear function fit and 95% confidence intervals at (**A**) a high latitude location (41.7°N) and (**B**) a low latitude location (23.0°N). Observations of the ratio of red fluorescence to biovolume for nanophytoplankton at 7 m from the Imaging FlowCytobot (IFCB) as a function of PAR calculated at 7 m depth (PAR(7 m)) with the nonlinear function fit and 95% confidence intervals at (**C**) a high latitude location (41.7°N) and (**D**) a low latitude location (32.2°N).

Derived E_{FT} values for the cruise transect (Fig. 5A) show similar patterns to the saturation parameter for photosynthesis, E_k, reported for the North Pacific (Uitz et al. 2008; Behrenfeld et al. 2016; Kulk et al. 2020). At the southernmost stations, calculated E_{FT} values range between 200 and 300 μmol photons m^{-2} s^{-1}, declining to 100–150 μmol photons m^{-2} s^{-1} near the transition zone. North of the chlorophyll front, E_{FT} values range between 25 and 100 μmol photons m^{-2} s^{-1}, indicative of low-light adapted phytoplankton communities. Experimental studies based on photosynthesis vs. irradiance curves have found E_k values of 238 ± 100 and 171 ± 98 μmol photons m^{-2} s^{-1} for waters with chlorophyll concentrations equivalent to the southern stations and the northern stations, respectively (Uitz et al. 2008) or regional values of 382 μmol photons m^{-2} s^{-1} in the NPSG and 70 μmol photons m^{-2} s^{-1} in the Eastern Pacific Subarctic Gyres Province (Kulk et al. 2020). It is important to note that in this study, E_{FT} was derived from estimates of fluorescence yield vs. PAR and was not spectrally corrected to photosynthetically usable radiation. Relative PAR calculated with respect to spectral phytoplankton pigment absorption at similar depths in open ocean conditions underestimates relative photosynthetically usable radiation by a factor of two (Laws et al. 1990), and would therefore lead to an underestimate of photosynthetically absorbed radiation at E_k values. This is apparent in Fig. 5A, where the Kulk et al. (2020) and Uitz et al. (2008) E_k values are between 1.5 and 2.5 times higher than the derived E_{FT} values from this study, whereas the Behrenfeld et al. (2016) measurements made with the daylength (DL) correction, which does not have this spectral correction, aligns much more closely with this study.

In addition, other caveats affect the E_{FT} estimates measured from underway systems. The clear-sky assumption for both the air–sea transmission and the derived PAR attenuation would lead to an underestimation of final PAR(7 m) values by up to 11% in entirely diffuse sky lighting conditions (*see* Supplemental Material), especially in the northern latitudes where cloudy conditions were more prevalent. There was also an implied assumption of no significant contribution to

backscattering by particles less than 0.2 μm as the AC-S and ECO Triplet were relatively calibrated by subtracting 0.2 μm-filtered seawater throughout the cruise. This would lead to an underestimation of PAR attenuation and an overestimation of PAR(7 m). The time for phytoplankton to reach the underway system (nominally about 10 s, given ship pipe layout and flow rate) and the duration of acquisition (up to 20 min for the IFCB) could allow for rapid and substantial relaxation of nonphotochemical quenching. However, over the course of each IFCB analysis, the fluorescence of nanophytoplankton did not significantly change for both a southern and northern station (*see* Supplemental Material). These uncertainties and resolutive limitations can be mitigated through the use of high throughput sensors (Swalwell et al. 2011; Olson et al. 2017) or autonomous profiling platforms such as BGC-Argo, which can monitor PAR at depth as well as measure fluorescence without the relaxation of nonphotochemical quenching. If the mixed layer depths are sufficiently deep, derivations of E_{FT} can be made as a function of depth in addition to time over the course of a day, yielding even higher spatial and temporal resolution observations.

Nevertheless, the consistency in the E_{FT} values observed under different cloud-cover conditions in the subtropical gyre and with varying PAR attenuation north of the transition zone chlorophyll front suggests that both the latitudinal trend and magnitude of E_{FT} in our present study are robust. Furthermore, using a similar approach to detect an irradiance-dependent depression of chlorophyll fluorescence from vertical profiles from the tropical Pacific, Cullen and Lewis (1995) found essentially the same pattern as in Fig. 4, but for the ratio of fluorescence to extracted chlorophyll, with an estimated threshold irradiance of 199 μmol photons m^{-2} s^{-1} PAR. This fluorescence light-dependence was comparable to that presented by Marra (1992) based on the diurnal variability of fluorescence. Finally, derived values of E_k as approximated from the Carbon : Chl ratio in Behrenfeld et al. (2016) with the additional incorporation of DL from the Silsbe et al. (2016) model (Fig. 5A) display latitudinal trends in their magnitude that are similar to the E_{FT} values of this study. Latitudinal matchups of the Behrenfeld et al. (2016) + DL E_k and the E_{FT} values from this study show a 1 : 1 relationship across most of the transect, with E_{FT} values increasing to 3 × E_k values in low-light adapted regions with cloudy conditions to the north (Fig. 6).

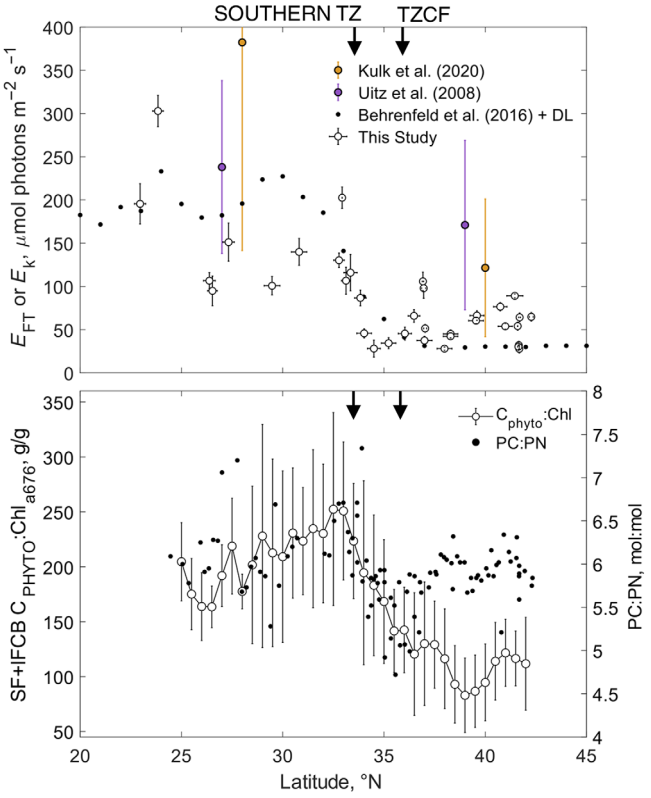

Fig. 5. (**A**) Latitudinal range of the fluorescence-irradiance threshold E_{FT} values derived from the nonlinear fit function, with 95% confidence interval error bars in the vertical as well as the range of latitudes the input measurements were collected from as horizontal error bars (white circles), as well as modeled values of the light saturation irradiance E_k calculated from the Behrenfeld et al. (2016) model using calculations of DL as described by Silsbe et al. (2016) with monthly MODIS data for the month of April 2019 from the OSU Ocean Productivity website (www.sites.science.oregonstate.edu/ocean.productivity/index.php) (black circles) and historical values of E_k and their standard deviations for the region from Uitz et al., 2008 (purple circles) and Kulk et al., 2020 (yellow circles) (**B**) latitudinal range in the phytoplankton carbon to chlorophyll ratio (C_{phyto} : Chl, white circles) and bulk particulate carbon to nitrogen ratio (PC : PN, black circles).

Ecological patterns in photophysiology

Changes in phytoplankton cell size or community composition may explain some of the observed shifts in

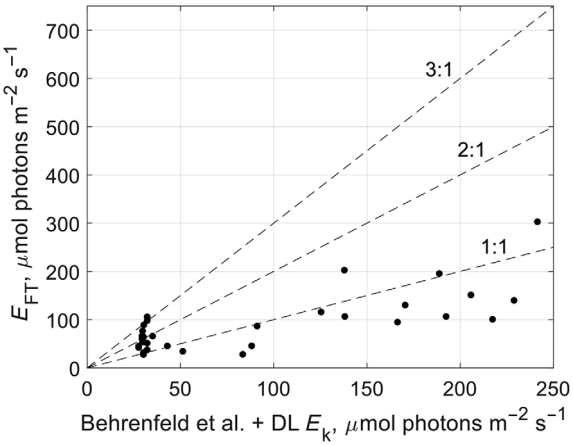

Fig. 6. Scatter plot of the light saturation irradiance (E_k) values derived using the Behrenfeld et al. (2016) method plus the DL correction from Silsbe et al. (2016) compared to derived fluorescence-irradiance threshold (E_{FT}) values from this study, matched up by latitude. Units for both are in μmol photons m^{-2} s^{-1}. Also plotted are the 1 : 1, 2 : 1, and 3 : 1 lines.

photoacclimation. Particle sizes changed over the course of the transect (Juranek et al. 2020), as measured by the pair of flow cytometers used in this study: SeaFlow (~ 0.5–6 μm) and the IFCB (~ 4–100 μm). The SeaFlow measured a shift in cell size across latitudes, associated with the small cyanobacterium *Prochlrococcus* (~ 0.5 μm) and *Synechococcus* (~ 1 μm), dominant in the subtropics and transition zone respectively, and relatively larger picoeukaryotes (~ 2–4 μm) at higher latitudes. In comparison, the IFCB showed a small shift in the mode of the size distribution (albeit this is based on equivalent spherical diameter, and thus does not account for shifts in cell shape), with values of 7.60, 7.45, and 6.48 μm in the subtropics, southern and northern transition zone, but a broadening of particle size northward (Juranek et al. 2020). The broadening of particle size distributions, and expected package effect, with latitude is inconsistent with the increase in Chl_{fl} : Chl_{a676} observed under low light, as larger cells tend to present lower pigment concentration and fluorescence yield relative to their size (Álvarez et al. 2017). The package effect scales to cell size for any given phytoplanktonic taxa (Nelson et al. 1993; Álvarez et al. 2017), hence the observed shifts in photoacclimation could be linked to species composition, rather than cell size. In fact, the changes in Chl_{fl} : Chl_{a676} ratios and E_{FT} are consistent with changes in taxonomy, as Juranek et al. (2020) reported that gymnodinoid dinoflagellates, which dominated both plankton biomass and abundance across the transect, were progressively replaced by small diatoms (*Thalassiosira* spp.) and coccolithophores (*Emiliania huxleyi*) in the northern transition zone waters. These taxonomic classes tend to be low-light adapted, with E_k values of 84 ± 11 and 115 μmol photons m^{-2} s^{-1} respectively and reach higher productivity at light saturation (Edwards et al. 2016), although strong adaptations have been noted for species in the genus *Thalassiosira* (Fisher et al. 2020).

Physiological and elemental stoichiometry is strongly related to factors governing primary production and growth rate (Behrenfeld et al. 2016; Inomura et al. 2020). Phytoplankton also reallocate their macromolecular content according to resource availability, growth rate, and environmental conditions (Elrifi and Turpin 1985; Healey 1985) which leads to significant variations in elemental composition. In the oligotrophic gyre, light-replete and nitrate-limited phytoplankton have reduced quotas of chlorophyll per cell, and subsequently a higher C_{PHYTO} : Chl ratio (Fig. 5A). In higher latitudes beyond the transition zone chlorophyll front, we observe lower C_{PHYTO} : Chl consistent with lower irradiance, higher nutrient supply, and faster growth rates (Geider 1987; Inomura et al. 2020). Figure 5B shows the latitudinal variability of the phytoplankton carbon-to-chlorophyll ratio, measured with the SeaFlow and IFCB, and the bulk ratio of particulate carbon to nitrogen. Ratios of phytoplankton carbon relative to total particulate organic carbon showed no significant latitudinal trend (values of 0.52 ± 0.10), though variability tended to increase at higher latitudes which could explain the small changes in the C : N stoichiometry relative to the absolute changes in C_{PHYTO} and C_{PHYTO} : Chl. We found that particulate C : N shows a very small decrease from the NPSG (6.0 ± 0.59) into the more productive zone north of the chlorophyll front (5.8 ± 0.36), $t(79) = 2.3$, $p < 0.05$ (Fig. 5) consistent with the general subtropical-to-subpolar trend observed in recent global data compilations (Martiny et al. 2013a; Galbraith and Martiny 2015). It is important to note, however, that for this transect we did not find evidence of iron limitation, especially in the northern stations, based on iron addition experiments. This latitudinal trend, although weak, likely reflects enhanced growth rates and increased protein : carbohydrate ratios of organic matter indicative of faster-growing phytoplankton north of the chlorophyll front (Martiny et al. 2013b; Inomura et al. 2020). The factor of three to five decrease in E_{FT} from the southern portion of the transect to the north corresponds to observations of net community production, measured underway using the O_2/Ar approach, which showed a factor of three increase over the transect (Juranek et al. 2020).

Conclusion

In this paper, continuous underway measurements of PAR, in vivo chlorophyll fluorescence, and chlorophyll absorption were used to follow a parameter characteristic of phytoplankton photoacclimation, like that of the saturation irradiance for photosynthesis, E_k, across a latitudinal gradient of light, nutrients, and temperature. This fluorescence-irradiance threshold, E_{FT}, developed by Comeau (2010) based on theory developed by Morrison (2003) and highlighted by Roesler and Barnard (2013) as a diagnostic, shows consistent latitudinal patterns with E_k approximations from other studies. Latitudinal patterns of E_{FT} also covary with other metrics consistent with changes in nutrient availability, growth rate, and the magnitude of primary productivity across the North Pacific. Specifically, both the particulate C : N ratio and the C_{PHYTO} : Chl ratio declined from south to north with the transition occurring just at the chlorophyll front where nutrient concentrations and production rates are elevated. In concert, we observe changes in resource allocation and photophysiology consistent with a transition from the nutrient poor, light-saturated NPSG to the more nutrient rich, lower light subpolar gyre. The observed trend in E_{FT} indicates phytoplankton acclimation to lower light levels north of the chlorophyll front, consistent with the presence of low-light adapted species. If it can be related quantitatively to the saturation irradiance for photosynthesis, this fluorescence threshold irradiance could become a useful optical signal that can be acquired in high resolution from a variety of moored and profiling platforms, providing valuable information on photophysiological patterns in sea surface phytoplankton assemblages and leading to improved models of marine primary productivity.

References

Álvarez, E., E. Nogueira, and Á. López-Urrutia. 2017. In vivo single-cell fluorescence and size scaling of phytoplankton chlorophyll content. Appl. Environ. Microbiol. **83**: e03317-16. doi:10.1128/AEM.03317-16

Babin, M., A. Morel, H. Claustre, A. Bricaud, Z. Kolber, and P. G. Falkowski. 1996. Nitrogen- and irradiance-dependent variations of the maximum quantum yield of carbon fixation in eutrophic, mesotrophic and oligotrophic marine systems. Deep-Sea Res. Part I Oceanogr. Res. Pap. **43**: 1241–1272. doi:10.1016/0967-0637(96)00058-1

Behrenfeld, M. J., and others. 2016. Revaluating ocean warming impacts on global phytoplankton. Nat. Clim. Change **6**: 323–330. doi:10.1038/nclimate2838

Behrenfeld, M. J., O. Prasil, M. Babin, and F. Bruyant. 2004. In search of a physiological basis for covariations in light-limited and light-saturated photosynthesis. J. Phycol. **40**: 4–25. doi:10.1046/j.1529-8817.2004.03083.x

Behrenfeld, M. J., T. K. Westberry, E. S. Boss, and others. 2009. Satellite-detected fluorescence reveals global physiology of ocean phytoplankton. Biogeosciences **6**: 779–794. doi:10.5194/bg-6-779-2009

Boss, E., and W. S. Pegau. 2001. Relationship of light scattering at an angle in the backward direction to the backscattering coefficient. Appl. Optics **40**: 5503–5507. doi:10.1364/AO.40.005503

Bouman, H. A., and others. 2018. Photosynthesis–irradiance parameters of marine phytoplankton: Synthesis of a global data set. Earth Syst. Sci. Data **10**: 251–266. doi:10.5194/essd-10-251-2018

Bowles, N. D., H. W. Paerl, and J. Tucker. 1985. Effective solvents and extraction periods employed in phytoplankton carotenoid and chlorophyll determinations. Can. J. Fish. Aquat. Sci. **42**: 1127–1131. doi:10.1139/f85-139

Buck, K. R., F. P. Chavez, and L. Campbell. 1996. Basin-wide distributions of living carbon components and the inverted trophic pyramid of the central gyre of the North Atlantic Ocean, summer 1993. Aquat. Microb. Ecol. **10**: 283–298. doi:10.3354/ame010283

Butler, W. L., and R. J. Strasser. 1977. Tripartite model for the photochemical apparatus of green plant photosynthesis. Proc. Natl. Acad. Sci. **74**: 3382–3385. doi:10.1073/pnas.74.8.3382

Cleveland, J. S., and M. J. Perry. 1987. Quantum yield, relative specific absorption and fluorescence in nitrogen-limited Chaetoceros gracilis. Mar. Biol. **94**: 489–497. doi:10.1007/BF00431395

Comeau, A. J. 2010. Examining temporal variations of phytoplankton photoacclimation using a novel fluorescence based approach. Masters thesis. Dalhousie Univ.

Côté, B., and T. Platt. 1983. Day-to-day variations in the spring-summer photosynthetic parameters of coastal marine phytoplankton. Limnol. Oceanogr. **28**: 320–344. doi:10.4319/lo.1983.28.2.0320

Cullen, J. J., A. M. Ciotti, R. F. Davis, and P. J. Neale. 1997. Relationship between near-surface chlorophyll and solar-stimulated fluorescence: Biological effects. Proc. Ocean Opt. XIII: 272–277. doi:10.1117/12.266454

Cullen, J. J., and M. R. Lewis. 1995. Biological processes and optical measurements near the sea surface: Some issues relevant to remote sensing. J. Geophys. Res. Oceans **100**: 13255–13266. doi:10.1029/95jc00454

Davis, R. F., C. C. Moore, J. R. V. Zaneveld, and J. M. Napp. 1997. Reducing the effects of fouling on chlorophyll estimates derived from long-term deployments of optical instruments. J. Geophys. Res. Oceans **102**: 5851–5855. doi:10.1029/96JC02430

Edwards, K. F., M. K. Thomas, C. A. Klausmeier, and E. Litchman. 2016. Phytoplankton growth and the interaction of light and temperature: A synthesis at the species and community level. Limnol. Oceanogr. **61**: 1232–1244. doi:10.1002/lno.10282

Elrifi, I. R., and D. H. Turpin. 1985. Steady-state luxury consumption and the concept of optimum nutrient ratios: A study with phosphate and nitrate limited *Selenastrum minutum* (chlorophyta). J. Phycol. **21**: 592–602. doi:10.1111/j.0022-3646.1985.00592.x

Falkowski, P. G., and J. A. Raven. 2007. Aquatic photosynthesis, 2nd ed.), STU-Student edition. Princeton Univ. Press.

Fisher, N. L., D. A. Campbell, D. J. Hughes, U. Kuzhiumparambil, K. H. Halsey, P. J. Ralph, and D. J. Suggett. 2020. Divergence of photosynthetic strategies amongst marine diatoms. PLoS One **15**: e0244252. doi:10.1371/journal.pone.0244252

Galbraith, E. D., and A. C. Martiny. 2015. A simple nutrient-dependence mechanism for predicting the stoichiometry of marine ecosystems. Proc. Natl. Acad. Sci. **112**: 8199–8204. doi:10.1073/pnas.1423917112

Geider, R. J. 1987. Light and temperature dependence of the carbon to chlorophyll a ratio in microalgae and cyanobacteria: Implications for physiology and growth of phytoplankton. New Phytol. **106**: 1–34. doi:10.1111/j.1469-8137.1987.tb04788.x

Geider, R. J., and H. L. MacIntyre. 2002. Physiology and biochemistry of photosynthesis and algal carbon acquisition, p. 44–77. *In* P. J. L. B. Williams, D. N. Thomas, and C. S. Reynolds [eds.], Phytoplankton productivity: Carbon assimilation in marine and freshwater ecosystems. Blackwell.

Geider, R. J., H. L. MacIntyre, and T. M. Kana. 1996. A dynamic model of photoadaptation in phytoplankton. Limnol. Oceanogr. **41**: 1–15. doi:10.4319/lo.1996.41.1.0001

Geider, R. J., H. L. MacIntyre, and T. M. Kana. 1998. A dynamic regulatory model of phytoplanktonic acclimation to light, nutrients, and temperature. Limnol. Oceanogr. **43**: 679–694. doi:10.4319/lo.1998.43.4.0679

Harrison, W. G., T. Platt, and M. R. Lewis. 1985. The utility of light-saturation models for estimating marine primary productivity in the field: A comparison with conventional

"simulated" in situ methods. Can. J. Fish. Aquat. Sci. **42**: 864–872. doi:10.1139/f85-110

Healey, F. P. 1985. Interacting effects of light and nutrient limitation on the growth rate of *Synechococcus linearis* (cyanophyceae). J. Phycol. **21**: 134–146. doi:10.1111/j.0022-3646.1985.00134.x

Holser, R. R., M. A. Goni, and B. Hales. 2011. Design and application of a semi-automated filtration system to study the distribution of particulate organic carbon in the water column of a coastal upwelling system. Mar. Chem. **123**: 67–77. doi:10.1016/j.marchem.2010.10.001

Inomura, K., A. W. Omta, D. Talmy, J. Bragg, C. Deutsch, and M. J. Follows. 2020. A mechanistic model of macromolecular allocation, elemental stoichiometry, and growth rate in phytoplankton. Front. Microbiol. **11**: 86. doi:10.3389/fmicb.2020.00086

Jassby, A. D., and T. Platt. 1976. Mathematical formulation of the relationship between photosynthesis and light for phytoplankton. Limnol. Oceanogr. **21**: 540–547. doi:10.4319/lo.1976.21.4.0540

Jolliff, J. K., R. W. Gould Jr., B. Penta, W. J. Teague, S. DeRada, F. P. Chavez, and R. A. Arnone. 2012. Water mass bio-optical properties in the Monterey Bay region: Fluorescence-based inference of shifts in phytoplankton photophysiology. J. Geophys. Res. Oceans **117**: C7. doi:10.1029/2011JC007568

Juranek, L. W., and others. 2020. The importance of the phytoplankton "middle class" to ocean net community production. Global Biogeochem. Cycles **34**: e2020GB006702. doi:10.1029/2020gb006702

Kiefer, D. A. 1973. Fluorescence properties of natural phytoplankton populations. Mar. Biol. **22**: 263–269. doi:10.1007/BF00389180

Kiefer, D. A., and R. A. Reynolds. 1992. Advances in understanding phytoplankton fluorescence and photosynthesis, p. 155–174. *In* P. G. Falkowski, A. D. Woodhead, and K. Vivirito [eds.], Primary productivity and biogeochemical cycles in the sea. Springer.

Kolber, Z., and P. G. Falkowski. 1993. Use of active fluorescence to estimate phytoplankton photosynthesis in situ. Limnol. Oceanogr. **38**: 1646–1665. doi:10.4319/lo.1993.38.8.1646

Kulk, G., and others. 2020. Primary production, an index of climate change in the ocean: Satellite-based estimates over two decades. Remote Sens. (Basel) **12**: 826. doi:10.3390/rs12050826

Laws, E. A., G. R. DiTullio, K. L. Carder, P. R. Betzer, and S. Hawes. 1990. Primary production in the deep blue sea. Deep-Sea Res. Part Oceanogr. Res. Pap. **37**: 715–730. doi:10.1016/0198-0149(90)90001-C

Lee, Z., K. Du, R. Arnone, S. Liew, and B. Penta. 2005. Penetration of solar radiation in the upper ocean: A numerical model for oceanic and coastal waters. J. Geophys. Res. Oceans **110**: C9. doi:10.1029/2004jc002780

Lewis, M. R., and J. C. Smith. 1983. A small volume, short-incubation-time method for measurement of photosynthesis as a function of incident irradiance. Mar. Ecol. Prog. Ser. **13**: 99–102. doi:10.3354/meps013099

Lynn, R. J. 1986. The subarctic and northern subtropical fronts in the eastern North Pacific Ocean in spring. J. Phys. Oceanogr. **16**: 209–222 doi:10.1175/1520-0485(1986)016<0209:TSANSF>2.0.CO;2

MacIntyre, H. L., J. J. Cullen, T. J. Whitsitt, and B. Petri. 2018. Enumerating viable phytoplankton using a culture-based Most Probable Number assay following ultraviolet-C treatment. J. Appl. Phycol. **30**: 1073–1094. doi:10.1007/s10811-017-1254-8

Maritorena, S., D. A. Siegel, and A. R. Peterson. 2002. Optimization of a semianalytical ocean color model for global-scale applications. Appl. Optics **41**: 2705–2714. doi:10.1364/AO.41.002705

Marra, J. 1992. Diurnal variability in chlorophyll fluorescence: Observations and modeling. *Ocean Optics XI*. Proceedings of the Ocean Optics XI. International Society for Optics and Photonics. 233–244.

Martiny, A. C., C. T. A. Pham, F. W. Primeau, J. A. Vrugt, J. K. Moore, S. A. Levin, and M. W. Lomas. 2013*a*. Strong latitudinal patterns in the elemental ratios of marine plankton and organic matter. Nat. Geosci. **6**: 279–283. doi:10.1038/ngeo1757

Martiny, A. C., K. Treseder, and G. Pusch. 2013*b*. Phylogenetic conservatism of functional traits in microorganisms. ISME J. **7**: 830–838. doi:10.1038/ismej.2012.160

Mason, J. D., M. T. Cone, and E. S. Fry. 2016. Ultraviolet (250–550 nm) absorption spectrum of pure water. Appl. Optics **55**: 7163–7172. doi:10.1364/AO.55.007163

Menden-Deuer, S., and E. J. Lessard. 2000. Carbon to volume relationships for dinoflagellates, diatoms, and other protist plankton. Limnol. Oceanogr. **45**: 569–579. doi:10.4319/lo.2000.45.3.0569

Mobley, C. D., and E. S. Boss. 2012. Improved irradiances for use in ocean heating, primary production, and photo-oxidation calculations. Appl. Optics **51**: 6549–6560. doi:10.1364/AO.51.006549

Moberg, E. A., and H. M. Sosik. 2012. Distance maps to estimate cell volume from two-dimensional plankton images. Oceanogr. Methods **10**. doi:10.4319/lom.2012.10.278

Moore, C. M., M. M. Mills, R. Langlois, A. Milne, E. P. Achterberg, J. L. Roche, and R. J. Geider. 2008. Relative influence of nitrogen and phosphorous availability on phytoplankton physiology and productivity in the oligotrophic sub-tropical North Atlantic Ocean. Limnol. Oceanogr. **53**: 291–305. doi:10.4319/lo.2008.53.1.0291

Morrison, J. R. 2003. In situ determination of the quantum yield of phytoplankton chlorophyll a fluorescence: A simple algorithm, observations, and a model. Limnol. Oceanogr. **48**: 618–631. doi:10.4319/lo.2003.48.2.0618

Nelson, N. B., B. B. Prézelin, and R. R. Bidigare. 1993. Phytoplankton light absorption and the package effect in California coastal waters. Mar. Ecol. Prog. Ser. **94**: 217–227.

Olson, R. J., A. Shalapyonok, D. J. Kalb, S. W. Graves, and H. M. Sosik. 2017. Imaging FlowCytobot modified for high throughput by in-line acoustic focusing of sample particles. Limnol. Oceanogr.: Methods **15**: 867–874. doi:10.1002/lom3.10205

Olson, R. J., and H. M. Sosik. 2007. A submersible imaging-in-flow instrument to analyze nano-and microplankton: Imaging FlowCytobot. Limnol. Oceanogr.: Methods **5**: 195–203. doi:10.4319/lom.2007.5.195

Parkhill, J.-P., G. Maillet, and J. J. Cullen. 2001. Fluorescence-based maximal quantum yield for psii as a diagnostic of nutrient stress. J. Phycol. **37**: 517–529. doi:10.1046/j.1529-8817.2001.037004517.x

Platt, T., and A. D. Jassby. 1976. The relationship between photosynthesis and light for natural assemblages of coastal marine phytoplankton. J. Phycol. **12**: 421–430. doi:10.1111/j.1529-8817.1976.tb02866.x

Platt, T., S. Sathyendranath, O. Ulloa, W. G. Harrison, N. Hoepffner, and J. Goes. 1992. Nutrient control of phytoplankton photosynthesis in the Western North Atlantic. Nature **356**: 229–231. doi:10.1038/356229a0

Pope, R. M., and E. S. Fry. 1997. Absorption spectrum (380–700 nm) of pure water. II. Integrating cavity measurements. Appl. Opt. **36**: 8710–8723. doi:10.1364/AO.36.008710

Ribalet, F., and others. 2019. SeaFlow data v1, high-resolution abundance, size and biomass of small phytoplankton in the North Pacific. Sci. Data **6**: 277. doi:10.1038/s41597-019-0292-2

Roden, G. I. 1971. Aspects of the transition zone in the Northeastern Pacific. J. Geophys. Res. **76**: 3462–3475. doi:10.1029/JC076i015p03462

Roesler, C. S., and A. H. Barnard. 2013. Optical proxy for phytoplankton biomass in the absence of photophysiology: Rethinking the absorption line height. Methods Oceanogr. **7**: 79–94. doi:10.1016/j.mio.2013.12.003

Sathyendranath, S., T. Platt, R. J. W. Brewin, and T. Jackson. 2019. Primary production distribution, p. 635–640. *In* J. K. Cochran, H. J. Bokuniewicz, and P. L. Yager [eds.], Encyclopedia of ocean sciences, 3rd ed. Academic Press.

Schuback, N., and P. D. Tortell. 2019. Diurnal regulation of photosynthetic light absorption, electron transport and carbon fixation in two contrasting oceanic environments. Biogeosciences **16**: 1381–1399. doi:10.5194/bg-16-1381-2019

Sharp, J. H. 1974. Improved analysis for particulate organic carbon and nitrogen from seawater. Limnol. Oceanogr. **19**: 984–989. doi:10.4319/lo.1974.19.6.0984

Silsbe, G. M., M. J. Behrenfeld, K. H. Halsey, A. J. Milligan, and T. K. Westberry. 2016. The cafe model: A net production model for global ocean phytoplankton. Global Biogeochem. Cycles **30**: 1756–1777. doi:10.1002/2016GB005521

Slade, W. H., E. Boss, G. Dall'Olmo, M. R. Langner, J. Loftin, M. J. Behrenfeld, C. Roesler, and T. K. Westberry. 2010. Underway and moored methods for improving accuracy in measurement of spectral particulate absorption and attenuation. J. Atmospheric Ocean. Technol. **27**: 1733–1746. doi:10.1175/2010JTECHO755.1

Strickland, J. D. H., and T. R. Parsons. 1972. A practical handbook of seawater analysis, 2nd ed. Fisheries Research Board of Canada.

Swalwell, J. E., F. Ribalet, and E. V. Armbrust. 2011. SeaFlow: A novel underway flow-cytometer for continuous observations of phytoplankton in the ocean. Limnol. Oceanogr.: Methods **9**: 466–477. doi:10.4319/lom.2011.9.466

Uitz, J., Y. Huot, F. Bruyant, M. Babin, and H. Claustre. 2008. Relating phytoplankton photophysiological properties to community structure on large scales. Limnol. Oceanogr. **53**: 614–630. doi:10.4319/lo.2008.53.2.0614

Wallen, D. G., and G. H. Geen. 1971. Light quality in relation to growth, photosynthetic rates and carbon metabolism in two species of marine plankton algae. Mar. Biol. **10**: 34–43. doi:10.1007/BF02026764

Zhang, X., L. Hu, and M.-X. He. 2009. Scattering by pure seawater: Effect of salinity. Opt. Express **17**: 5698–5710. doi:10.1364/OE.17.005698

Acknowledgments

We are grateful for the sea-going support from marine technicians and the crew of the *R/V Kilo Moana*, without which this work would not have been possible. This work was inspired by the work of Dr. John Cullen who also kindly provided helpful comments on the manuscript. We thank Tully Rohrer for technical expertise. We also thank the editors and two anonymous reviewers for their insightful comments and suggestions. This work was primarily supported by Simons Foundation awards 329104 to A.E.W. All data have been uploaded to Zenodo.org (10.5281/zenodo.5178649) and are freely available at the Simons Collaborative Marine Atlas Project (https://simonscmap.com/).

Conflict of Interest

None declared.

Submitted 11 August 2021
Revised 23 November 2021
Accepted 11 January 2022

Associate editor: David Antoine